Shock-induced wave propagation over porous and fractured borehole zones: Theory and experiments

Huajun Fan
Faculty of Civil Engineering and Geosciences, Department of Geoscience and Engineering, Delft University of Technology, Stevinweg 1, 2628 CN Delft, The Netherlands

D. M. J. Smeulders[a)]
Department of Mechanical Engineering, Eindhoven University of Technology, P.O. Box 513, 5600 MB Eindhoven, The Netherlands

(Received 8 January 2013; revised 23 June 2013; accepted 13 August 2013)

Borehole waves are strongly affected by adjacent porous zones or by fractures intersecting the borehole. A theoretical description for both porous and fracture zones is possible based on the introduction of an effective borehole fluid bulk modulus, characterizing the wave attenuation via borehole wall impedance. This impedance can be calculated for both porous and fracture zones adjacent to the borehole, thus predicting borehole wave attenuation, transmission, and reflection over such zones. A shock tube setup generates borehole tube waves that are used for porous and fracture zone characterization. A PVC sample is used to introduce and vary fractures in a cylindrical sample. Shock wave experiments show that attenuation in boreholes adjacent to porous zones can be predicted by theory. The transmittivities of a borehole tube wave over 1 and 5 mm fractures are correctly predicted, thus showing the potential of borehole wave experiments for fracture detection and characterization. © *2013 Acoustical Society of America*. [http://dx.doi.org/10.1121/1.4826950]

PACS number(s): 43.35.Pt, 43.58.Bh, 43.40.Sk [KVH] Pages: 4792–4800

I. INTRODUCTION

The Stoneley wave has been used to detect and characterize fracture zones.[1–5] In the horizontal fracture case, Stoneley waves are attenuated because of flow into the fracture and scattering by the fracture.[6] The fracture zone is traditionally modeled as a fluid-filled narrow parallel-plate channel in which fracture waves propagate. These fracture waves carry part of the energy of the borehole wave radially outward away from the borehole and thus attenuate the borehole wave itself. If the viscous skin depth of the fracture wave is on the order of the fracture aperture, these fracture waves are also attenuated by viscous effects, and thus some of the energy of the borehole wave is dissipated. Moreover, because the fracture zone is experienced by the borehole Stoneley wave as a zone with a contrast in borehole impedance, Stoneley wave reflection and transmission will be induced. The reflected Stoneley waves carry information about the size, shape, and orientation of the fracture and are thus of potential interest for fractured reservoir characterization.

In this paper, first theory and application of Stoneley wave propagation in a single horizontal fracture plane are discussed. Next we describe the shock tube facility. This facility was used previously to detect borehole surface wave modes,[7–10] and is comparable with the setup used by Winkler *et al*.[11] Measurements of the wave experiments in the shock tube are presented and discussed. Finally, conclusions are drawn.

[a)]Author to whom correspondence should be addressed. Electronic mail: d.m.j.smeulders@tudelft.nl

II. THEORETICAL FORMULATION

We consider a borehole (radius R) intersected by a horizontal plane fracture (aperture h). Cylindrical coordinates r, z are used, where r is the radial distance from the borehole center, and z is the vertical coordinate pointing downward. The center plane of the fracture is at $z = 0$. We assume that the experiments are carried out at frequencies lower than the cutoff frequency of any mode other than of the fundamental tube wave, thus the borehole fluid pressure is considered uniform across the borehole. The wave equation is given by

$$\frac{d^2\psi}{dz^2} + \kappa^2\psi = 0, \tag{1}$$

where ψ is the wave displacement potential and κ is the axial wavenumber. In the region $z > h/2$ and $z < -h/2$, the wavenumber is expressed as κ_1, and in the layer where $-h/2 < z < h/2$, the wavenumber is κ_2.

The fluid pressure p and the axial displacement U are given as follows:

$$p = \rho_f \omega^2 \psi, \tag{2}$$

$$U = \frac{d\psi}{dz}, \tag{3}$$

where ρ_f is the fluid density and ω is the angular frequency. We now consider wave propagation and reflection in the borehole. Wave propagation is described by

$$\psi = A^+ e^{-i\kappa_1 z} + A^- e^{i\kappa_1 z} \quad \text{for} \quad z < -\frac{1}{2}h, \tag{4}$$

 0001-4966/2013/134(6)/4792/9/$30.00

$$\psi = B^+ e^{-i\kappa_2 z} + B^- e^{i\kappa_2 z} \quad \text{for} \quad -\frac{1}{2}h < z < \frac{1}{2}h, \tag{5}$$

$$\psi = C^+ e^{-i\kappa_1 z} \quad \text{for} \quad z > \frac{1}{2}h. \tag{6}$$

In the region $z < -h/2$, where $A^+ e^{-i\kappa_1 z}$ represents the incident wave propagating in the positive z direction and A^+ is the incident amplitude coefficient, $A^- e^{i\kappa_1 z}$ is the reflected wave propagating in the negative z direction and A^- is the reflected amplitude coefficient. In the region $-h/2 < z < h/2$, B^+ and B^- are the amplitude coefficients for waves propagating in the positive z and negative z directions, respectively. In the region $z > h/2$, C^+ is the amplitude coefficient of the transmitted waves. As for the boundary conditions, at $z = h/2$ and $z = -h/2$, the fluid displacement and the pressure should be continuous. We then obtain the coefficients A^-, B^+, B^-, and C^+ as a function of the incident amplitude coefficient term A^+:

$$A^-/A^+ = -2i(\kappa_2^2 - \kappa_1^2)\sin(\kappa_2 h)/G, \tag{7}$$

$$B^+/A^+ = 2\kappa_1(\kappa_1 + \kappa_2)e^{i\kappa_2 h}/G, \tag{8}$$

$$B^-/A^+ = 2\kappa_1(\kappa_2 - \kappa_1)e^{-i\kappa_2 h}/G, \tag{9}$$

$$C^+/A^+ = 4\kappa_1\kappa_2 e^{i\kappa_1 h}/G, \tag{10}$$

where G is given by

$$G = (\kappa_1 + \kappa_2)^2 e^{i\kappa_2 h} - (\kappa_1 - \kappa_2)^2 e^{-i\kappa_2 h}. \tag{11}$$

The above equations were also found by Tang and Cheng.[12] In the upper zone, i.e., the zone above the fracture, the pressure in the borehole is given by

$$\hat{p} = \rho_f \omega^2 A^+ [e^{-i\kappa_1 z} + (A^-/A^+)e^{i\kappa_1 z}], \tag{12}$$

where the ratio A^-/A^+ is defined by Eq. (7). Using the boundary condition that $\hat{p}$ is $\hat{p}_0$ at $z = -d$, where d is the distance between the sample top and the fracture center, yields

$$\hat{p} = \hat{p}_0 \frac{[e^{-i\kappa_1 z} + (A^-/A^+)e^{i\kappa_1 z}]}{[e^{i\kappa_1 d} + (A^-/A^+)e^{-i\kappa_1 d}]}, \tag{13}$$

in the upper zone. In the lower zone (below the fracture), we have that

$$\hat{p} = \hat{p}_0 \frac{C^+}{A^+} \frac{e^{-i\kappa_1 z}}{[e^{i\kappa_1 d} + (A^-/A^+)e^{-i\kappa_1 d}]}, \tag{14}$$

where the ratio C^+/A^+ is defined by Eq. (10).

III. BOREHOLE IMPEDANCE

A. Formation impedance

In the borehole, the wave propagation is defined by an effective fluid bulk modulus:[13]

$$\frac{1}{K_{\text{eff}}} = \frac{1}{K_f} + \frac{1}{G} + \frac{2}{i\omega R Z_R}, \tag{15}$$

where K_f is the fluid bulk modulus, G is the shear modulus of the formation, and Z_R is the wall impedance, describing the pressure-velocity ratio at the borehole wall. It can be expressed as[13]

$$\frac{1}{Z_R} = \frac{k_0}{\eta R}\kappa_r R \frac{K_1(\kappa_r R)}{K_0(\kappa_r R)}, \tag{16}$$

where k_0 is the permeability of the formation, η is the viscosity of the fluid, and K_1 and K_0 are modified Bessel functions of first and zeroth order, respectively. In the above equation, the radial wavenumber κ_r is given by

$$\kappa_r^2 = -i\omega/D_h, \tag{17}$$

for incompressible dynamic (Darcy) fluid motion in a rigid formation. $D_h = k_0 K_f/(\eta\phi)$ is the hydraulic diffusivity, with ϕ the porosity of the formation. As indicated by Kostek *et al.*,[3] for wave propagation in the fracture, κ_r can simply be computed from $\sqrt{\alpha(\omega)}\omega/c_f$, where c_f is the fluid wave speed and $\alpha(\omega)$ is the dynamic tortuosity as defined by Johnson *et al.*[14] Therefore, in the limiting case for low frequencies, we have that

$$\lim_{\omega\to 0} \frac{\sqrt{\alpha(\omega)}\omega}{c_f} = -\frac{i\omega}{D_h}. \tag{18}$$

Here we have assumed that the attenuation of the borehole wave is governed by viscous effects due to the oscillatory radial "breathing" fluid motion, where the elasticity of the formation is of minor importance. The elasticity, however, cannot be ignored in the expression for the effective borehole fluid bulk modulus (15). We have to note that this approach [Eqs. (15), (16), and (17)] is only valid for low frequencies, where the Stoneley wave becomes a tube wave. The wavenumber and velocity of the tube wave are now easily given by

$$\kappa = \frac{\omega}{c_T} = \omega\sqrt{\frac{\rho_f}{K_{\text{eff}}}}. \tag{19}$$

For a borehole radius of 10 cm, a fluid bulk modulus $K_f = 2.0$ GPa, and a fluid density is $\rho_f = 1000$ kgm^{-3}, we compute the phase speed and the attenuation of the tube wave as a function of frequency, for three different porosity-permeability combinations. For the shear modulus we use $G = 3.0$ GPa. Results are plotted in Fig. 1. Curves "a" refer to a porosity of 16% and a permeability of 10 mD, curves "b" to a porosity of 20% and a permeability of 100 mD, and curves "c" to the highest values for porosity and permeability of 26% and 1000 mD, respectively. The dependence on porosity and permeability is clearly visible. The higher the permeability, the more attenuation is observed due to the increased oscillatory infiltration into the formation ("breathing"). In the high-frequency limit, the impedance term tends to zero, so that the effective bulk modulus simply becomes $1/K_{\text{eff}} = 1/K_f + 1/G$. If also the inverse shear modulus would vanish, we retrieve the relation $K_{\text{eff}} = K_f$, so that the tube wave velocity equals the fluid wave speed c_f.

B. Fracture impedance

In this case, the wall impedance is defined by averaged parameters over the fracture aperture h:

$$Z_R = \frac{\langle p(R,z)\rangle}{\langle v(R,z)\rangle}, \tag{20}$$

where $p(R,z)$ is the fluid pressure at the fracture opening and $v(R,z)$ is the radial velocity of the fluid along the fracture opening. The notation $\langle\cdot\rangle$ denotes averaging over the domain $[-h/2 < z < h/2]$, at $r = R$. Thus, the velocity and pressure distribution in the fracture need be known. It was found by Tang and Cheng[6] that

$$v_r(r,z) = -H_1(\kappa_r r)[A\kappa_r\cos(fz) + D\bar{f}\cos(\bar{f}z)], \tag{21}$$

$$v_z(r,z) = H_0(\kappa_r r)[-fA\sin(fz) + D\kappa_r\sin(\bar{f}z)], \tag{22}$$

$$p(r,z) = \frac{-i\omega\rho_f A}{1+\frac{4}{3}i\omega\nu/c_f^2}H_0(\kappa_r r)\cos(fz), \tag{23}$$

where H_0 and H_1 are Hankel functions of zeroth order and first order, respectively, and $\nu = \eta/\rho_f$ is the kinematic viscosity. A and D are dimension-full arbitrary constants. The modified wavenumbers f and $\bar{f}$ are expressed as follows:

$$f^2 = \frac{\omega^2}{c_f^2 + \frac{4}{3}i\omega\nu} - \kappa_r^2, \tag{24}$$

$$\bar{f}^2 = \frac{\omega}{i\nu} - \kappa_r^2. \tag{25}$$

The wavenumber κ_r in the fracture is given by the dispersion equation[6]

$$\kappa_r^2\tan\left(\frac{h}{2}\bar{f}\right) + f\bar{f}\tan\left(\frac{h}{2}f\right) = 0. \tag{26}$$

This equation is solved numerically, and the resulting pressure and velocity field in the fracture is obtained from Eqs. (21) and (23). Next, averaging over the fracture opening is performed and the fracture impedance is calculated from Eq. (20):

$$Z_R = \frac{i\kappa_r c_f^2\rho_f H_0(\kappa_r R)}{\omega H_1(\kappa_r R)}. \tag{27}$$

The effective bulk modulus and hence the borehole wavenumber are now known from Eqs. (15) and (19). Other, perhaps more complete theories have been derived by Korneev,[15,16] who relaxes the assumption of wall rigidity in the derivation of the dispersion equation for fracture waves.

IV. EXPERIMENTAL SETUP

The vertical shock tube is shown in Fig. 2. It is 7.44 m long and consists of a high-pressure section and a low-pressure section, separated by a diaphragm. The wall thickness of the tube is 2.5 cm. The shock tube was also used for other borehole measurements in the past.[7,8] The dimensions of the sections are indicated in Fig. 2. A cylinder with a centralized borehole is mounted in the test section of the shock tube and saturated with water. The length of the cylinder is L. It has a single horizontal fracture intersecting the borehole. A miniature pressure transducer is mounted in a probe (P2), so that it can be positioned along the axial direction of the borehole. In order to enhance the excitation of borehole waves and suppress body wave generation in the sample itself, an acoustic funnel (see inset of Fig. 2) is installed approximately 1 mm above the top of the sample, consisting of a thick-walled cylinder with decreasing internal cross-sectional open area in the downward direction.

A wave experiment proceeds as follows: The pressure in the high pressure section is increased to 1 to 5 bars. Rupture of the diaphragm is caused by means of an electric current pulse. A shock wave in air is generated which travels downward and is transmitted into the water layer (see Fig. 2). The wave is partially reflected and partially transmitted into the funnel and the borehole. The pressure at different positions inside the borehole is measured by P2. The shock tube wall is equipped with pressure transducer P1, which is used to

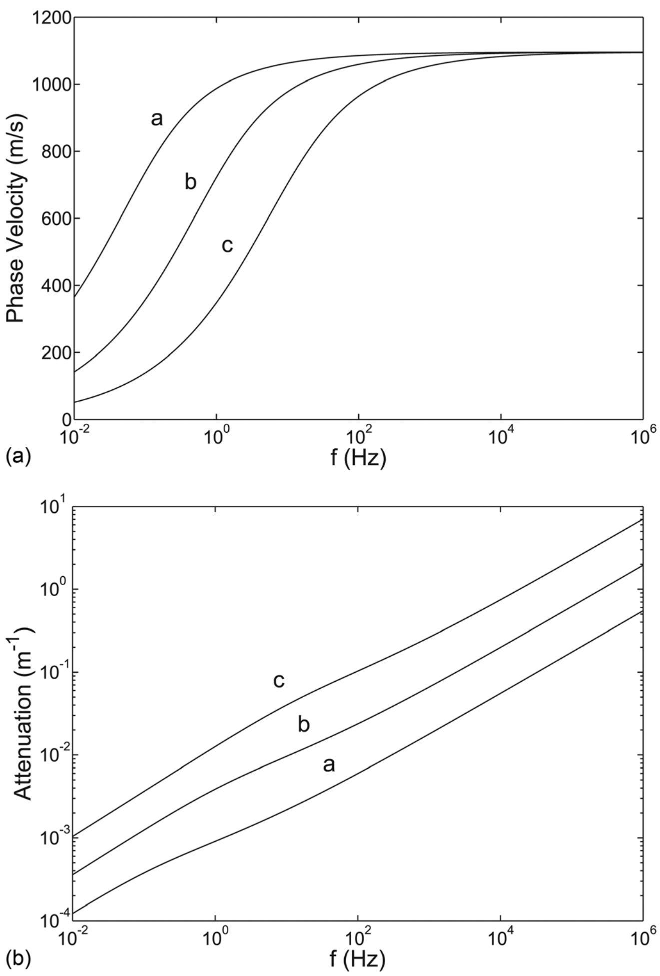

FIG. 1. Phase velocity and attenuation of the tube wave along a porous formation. a: $k_0 = 10$ mD, $\phi = 16\%$, b: $k_0 = 100$ mD, $\phi = 20\%$, c: $k_0 = 1000$ mD, $\phi = 26\%$.

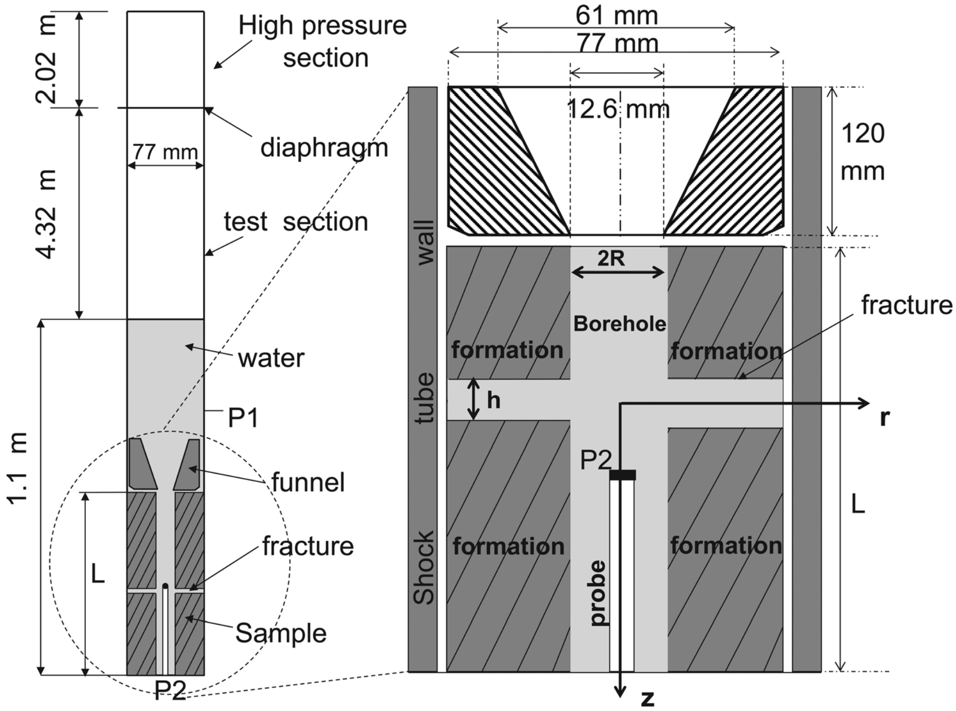

FIG. 2. Schematic of the shock tube setup. An acoustic funnel is installed on top of the sample for borehole wave enhancement (see inset for details).

trigger the data acquisition system. By repeating the wave experiments, we can measure the full pressure profiles in the borehole.

V. EXPERIMENT RESULTS

In order to determine the effect of the funnel on the input signal, we measured the pressure development in the funnel by means of sensor P2. The results are shown in Fig. 3. We notice that the pressure profile gradually evolves from the step-like input signal (a) above the funnel toward a more oscillatory pattern (c), where the distance between peak and trough corresponds with the funnel length. The signal (c) measured just below the funnel is used as input signal p_0 for the borehole wave computations described in Sec. II. Conventional fast Fourier transformation (FFT) is used to convert the temporal signal p_0 to the frequency signal $\hat{p}_0$.

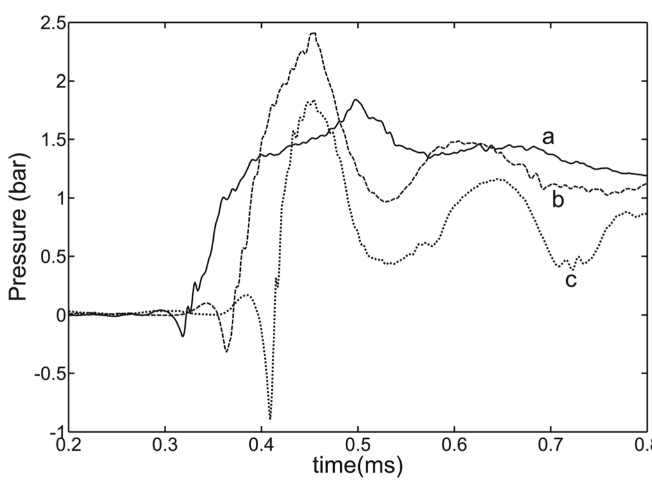

FIG. 3. Development of the measured pressure profile in the funnel: 5 mm above the funnel (a), in the middle of the funnel (b), and 1 mm below the funnel (c).

A. Borehole fractures

A PVC cylinder (with diameter 76.5 mm) in which a borehole (with diameter 12.2 mm) was drilled, is cut into two pieces. By positioning one piece on top of the other but slightly apart, a horizontal slit between the two pieces is generated which can be varied in aperture h by means of separator poles. The length of the upper piece is 396 mm, the lower piece is 195 mm. The three separator poles are arranged at 120° azimuths. The slit aperture can be changed by using different lengths of the poles. The borehole, fracture, and shock tube are carefully saturated with water. The properties of the PVC sample are in Table I.

We start with experiments where $h = 1$ mm. Probe P2 was consecutively displaced over 5 mm distances between 329 and 434 mm from the sample top. In this interval 23 shock wave experiments were carried out. The resulting microseismogram is shown in Fig. 4. The tube wave is clearly visible (St). The slope of the line St connecting all first arrivals of the tube waves in Fig. 4 corresponds with a tube wave speed of 960 ± 40 m/s. In Fig. 4, also fluid wave mode E1 is indicated which propagates with a speed of 1500 m/s. The identification of the different wave modes was performed by using the so-called semblance cross correlation method.[17] This method picks wave arrivals by computing the scalar semblance in a time window for a large number of possible arrival times and slownesses. The maximum values of semblance are interpreted as arrivals and their associated slownesses are plotted in a slowness-time

TABLE I. Properties of the samples.

Sample	L (mm)	ϕ (%)	k_0 (D)	K_b (GPa)	G (GPa)	ρ_b (kg/m^3)	ρ_s (kg/m^3)
PVC	591 + h	0	0	7.8	1.7	1427	1427
Porous	348	47.6	15 ± 2	7.1	3.0	1310	2495

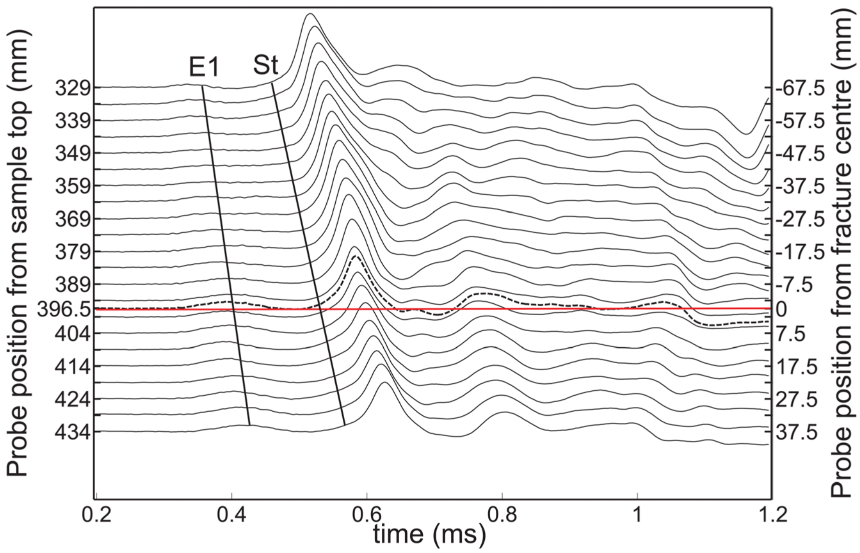

FIG. 4. (Color online) Microseismogram comprising 23 shock wave experiments in the PVC sample. The fracture center is at 396.5 mm from the sample top. The fracture aperture is 1 mm. The line St connects first arrivals of the Stoneley wave. E1 is the fluid wave arriving earlier than the Stoneley wave and having a velocity of 1500 m/s.

coherence graph in Fig. 5. In Fig. 5, the different colors stand for the different values of the coherence. The value is from 0 (black) to 100 (white), which means that in the black area there is no coherence and in the white area the coherence is maximal. In Fig. 5, there is also a coherence plot maximum E2 that cannot clearly be distinguished in the microseismogram (Fig. 4).

Two selected pressure recordings are compared with theory in Fig. 6. In Fig. 6(a), the position of the transducer is 67.5 mm above the fracture center. In Fig. 6(b), the position of the transducer is 27.5 mm below the fracture center. In Fig. 6(a), the agreement between experiment and theory is very good. The amplitude of the first peak perfectly matches theory. Note that the theoretical result stems from Eqs. (13) and (14), followed by a standard inverse FFT routine to convert the signals back to the temporal domain. The input parameters for the theory were obtained from independent laboratory experiments and no data fitting procedure was applied. The pressure trough A is not measured. It is associated with precursor tube mode[18] in the input signal p_0 (Fig. 3). In Fig. 6(b), where we compare theory and experiment at some distance below the fracture, the agreement between experiment and theory is even better. We note that in Figs. 6(a) and 6(b) event E1 does not appear in

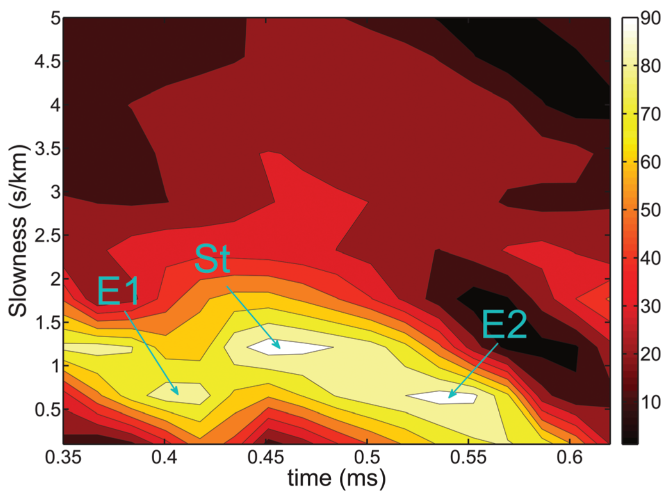

FIG. 5. Coherence plot for wave identification within the PVC sample. Event E1 is the fluid wave arriving earlier than the Stoneley wave (St) and having a velocity of 1500 m/s. E2 is a second fluid wave event that cannot clearly be identified in the microseismogram.

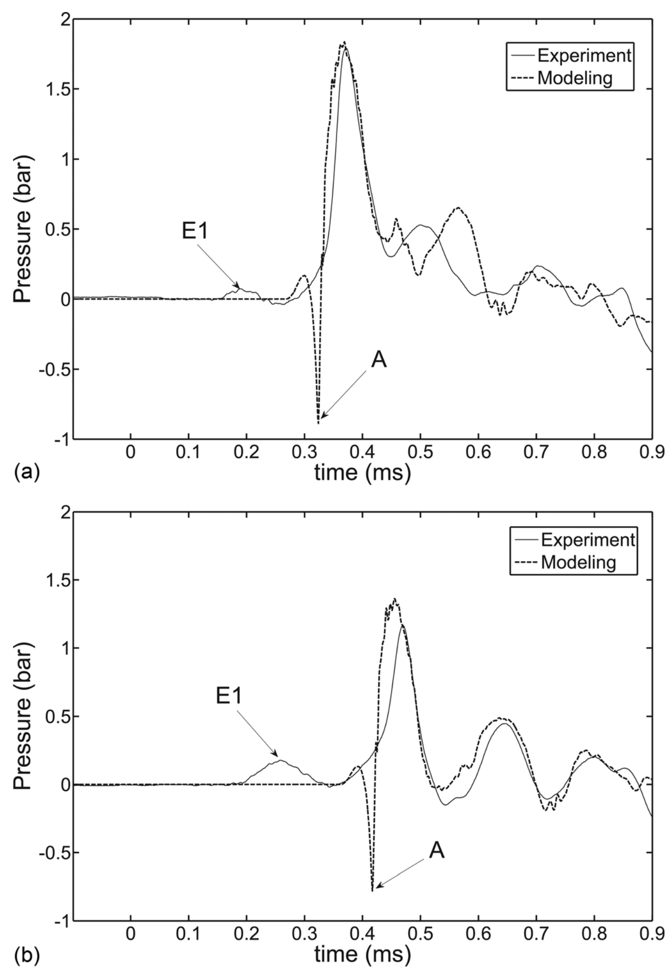

FIG. 6. Experimental and modeled pressure signals in the PVC sample with 1 mm fracture aperture at 67.5 mm above the fracture center (a), and 27.5 mm below the fracture center (b). E1 is the fluid wave arriving earlier than the Stoneley wave (St) and having a velocity of 1500 m/s. The precursor mode A is also visible.

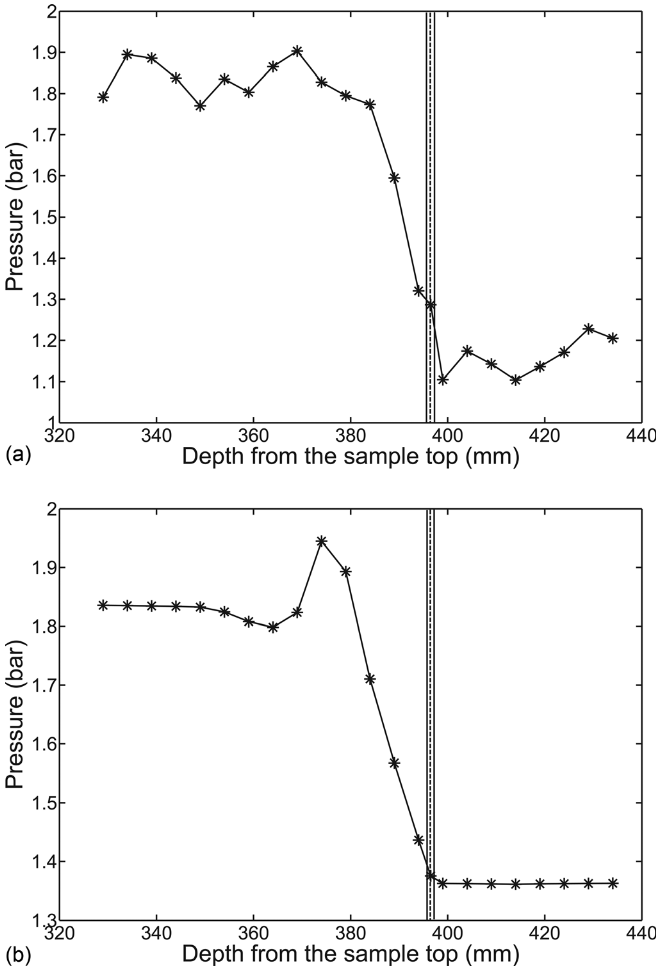

FIG. 7. Amplitude of the Stoneley wave at different positions in the borehole of the PVC sample with 1 mm fracture. The dashed vertical line is the center of the fracture and the two solid lines are the borders of the fracture. (a) Experiment, (b) theory.

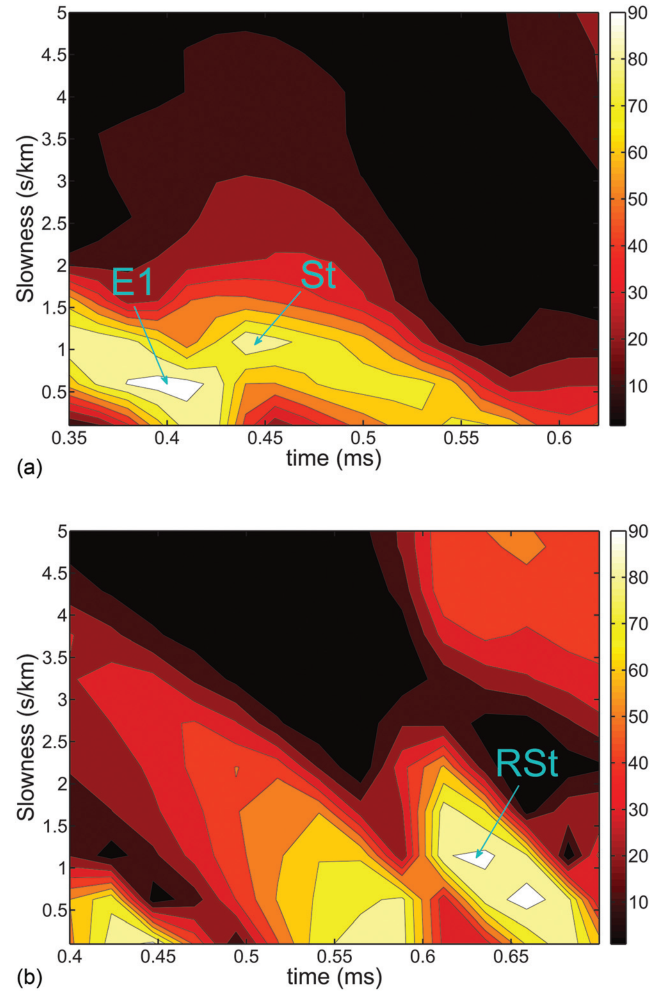

FIG. 9. Coherence plots for wave transmission (a) and wave reflection (b) within the PVC sample. The fracture aperture is 5 mm. Events E1, St, and RSt can clearly be identified.

the theoretical prediction. This is because E1 is associated with a fluid bulk mode that is not part of the theoretical description given in Sec. II.

Next, all amplitudes of the tube waves are compared with theory in Fig. 7. These amplitudes are the maximum pressure values in all 23 snapshots. In both Figs. 7(a) and 7(b), the vertical lines represent the fracture position. We note that there is a strong decrease in amplitude caused by the presence of the fracture. Surprisingly, the decrease in amplitude starts somewhat earlier than where the fracture is

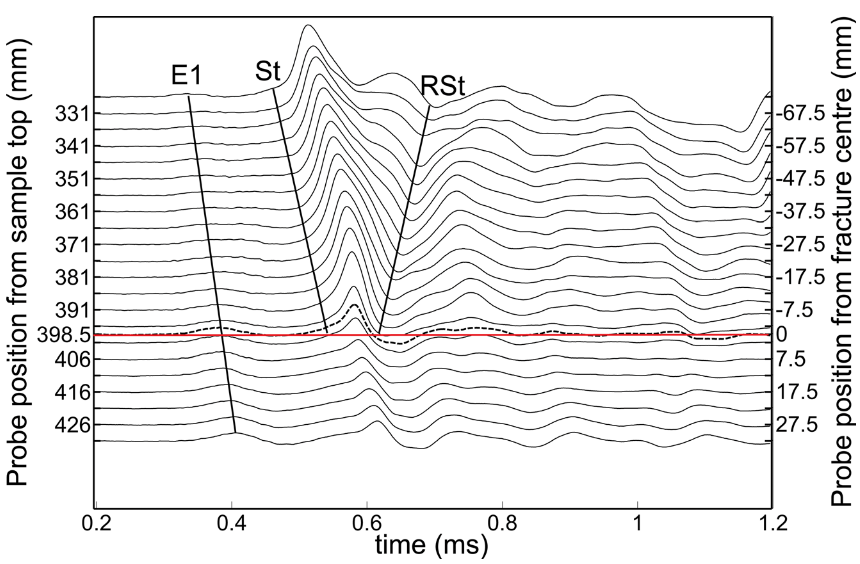

FIG. 8. (Color online) Microseismogram comprising 23 shock wave experiments in the PVC sample. The fracture center is at 398.5 mm from the sample top. The fracture aperture is 5 mm. The line St connects first arrivals of the Stoneley wave; the line RSt connects the inflection points representing the reflected Stoneley wave. E1 is the fluid wave arriving earlier than the Stoneley wave and having a velocity of 1500 m/s.

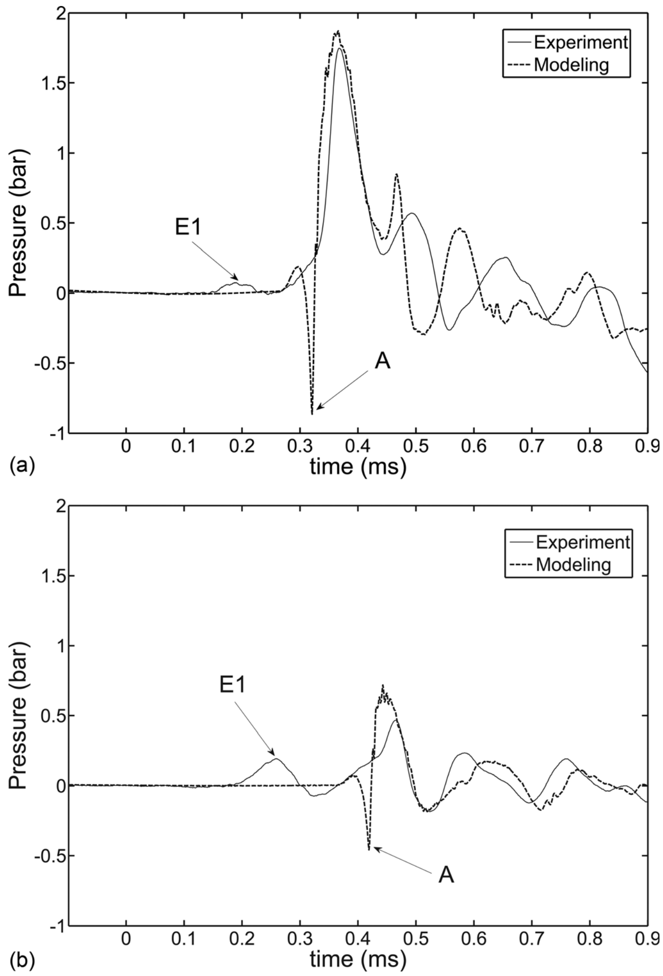

FIG. 10. Experimental and modeled pressure signals in the PVC sample with 5 mm fracture aperture at 72.5 mm above the fracture center (a), and 27.5 mm below the fracture center (b). E1 is the fluid wave, and A is the precursor pressure trough.

located. In Fig. 7(b), the modeled amplitude also predicts this sharp decrease over the fracture very well. The pressure level before pressure decay (1.8 bar) is in agreement with theory. The pressure level after pressure decay is around 1.2 bar for the experiment and around 1.4 bar for the modeling. This means that the tube wave loses somewhat more energy over the fracture in the experiment than predicted by theory.

Next, new separator poles were used to obtain a fracture aperture of 5 mm. The center of the fracture is now at 398.5 mm from the sample top. Again, 23 shock wave experiments were carried out. The resulting microseismogram is shown in Fig. 8. Apart from the arriving tube wave, also a reflection from the fracture can now be distinguished. The line St again connects all first arrivals of the tube wave. The velocity is determined to be 960 ± 40 m/s, which is in agreement with the previous velocity measurements. The dotted horizontal line indicates the position of the fracture. The slowness-time coherence is plotted in Fig. 9. In Fig. 9(a), besides the arrival of the Stoneley wave, again event E1 can be identified. The reflected Stoneley wave is identified in the slowness-time coherence Fig. 9(b).

Again, two snapshots are compared with theory in Fig. 10. In Fig. 10(a), the position of the transducer is 72.5 mm above the fracture center. In Fig. 10(b), the position of the transducer is 27.5 mm below the fracture center. In Fig. 10(a), the amplitude of the first peak is perfectly predicted by theory, and also the gradual oscillatory pressure decrease, albeit some time lag between predicted and recorded peaks and troughs. Note that also reflectivity from the fracture is included in the theory (see Sec. II). In Fig. 10(b), where we compare theory and experiment at some distance below the fracture, the agreement between experiment and theory is also good. Again, event E1 does not appear in the theoretical prediction because E1 is associated with a bulk water mode that is not part of the theoretical description given in Sec. II. It can be seen in Fig. 10(b) that the first peak of the Stoneley wave is slightly overpredicted by theory. By comparing Fig. 10(b) with Fig. 6(b), we find that the Stoneley wave amplitude decreases much more over the 5 mm fracture than over the 1 mm fracture.

The amplitudes of the tube waves are compared with theory in Fig. 11. For 23 traces, the maximum amplitude was determined and plotted in Fig. 11. We note that there is a strong decrease in amplitude caused by the presence of the 5 mm fracture. This decrease is larger than for the 1 mm fracture case. The pressure level before pressure decay is

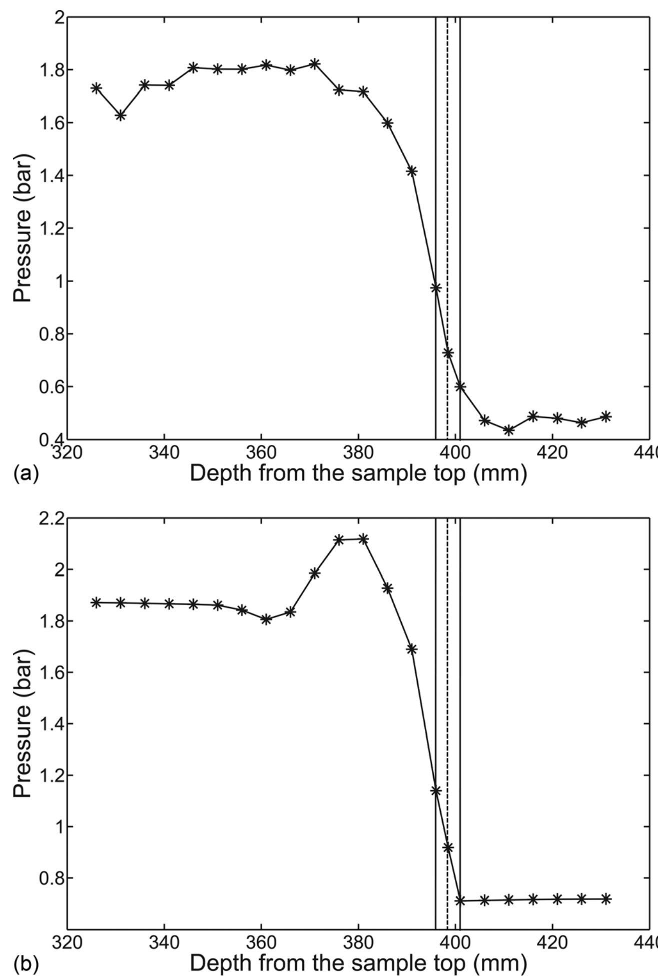

FIG. 11. Amplitude of the Stoneley wave at different positions in the borehole of the PVC sample with 5 mm fracture. The dashed vertical line is the center of the fracture and the two solid lines are the borders of the fracture. (a) Experiment, (b) theory.

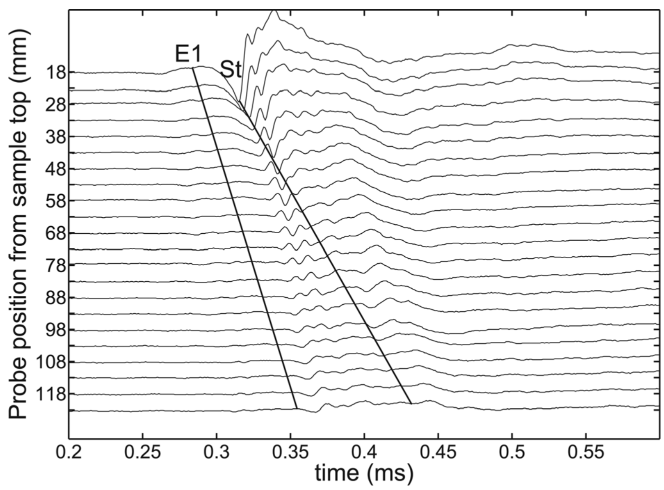

FIG. 12. Microseismogram comprising 22 shock wave experiments in the porous sample. The line St connects the first arrivals of the Stoneley wave. E1 is the fluid wave traveling with a speed of 1500 m/s.

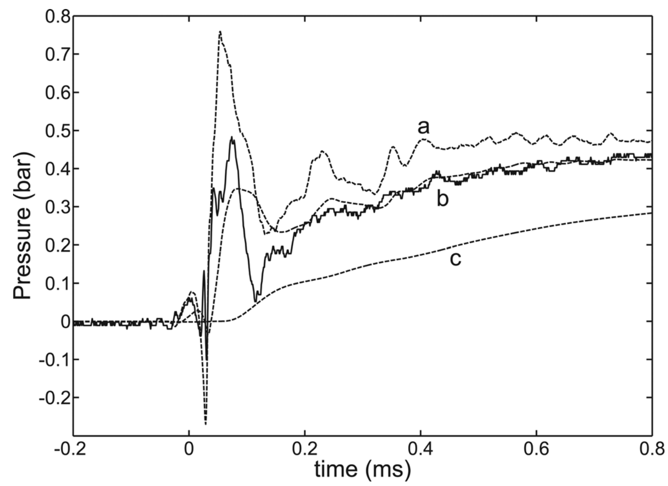

FIG. 14. Experimental and modeled pressure signals in the porous sample at 48 mm from the sample top. Three different permeabilities 0.5 D (a), 5 D (b), and 50 D (c) are used for the modeling.

perfectly predicted by theory again. The pressure level after pressure decay is around 0.5 bar for the experiment and around 0.7 bar for the modeling. This again shows that the tube wave loses somewhat more energy over the fracture in the experiment than predicted by theory.

B. Porous sample

Next, we use a porous sample for tube wave attenuation measurements. No fracture is present here. The length of the sample is 348 mm, the borehole diameter is 12.5 mm, and the outer sample diameter is 76.8 mm. The properties of the porous sample are given in Table I. Probe P2 was consecutively displaced over 5 mm distances from 18 to 123 mm from the sample top. In this interval 22 shock wave experiments were carried out. The resulting microseismogram is shown in Fig. 12. The slope of the line St connecting all first arrivals of the tube waves in Fig. 12 corresponds with a wave speed of 905 ± 40 m/s. The slowness-time coherence is given in Fig. 13. In Fig. 13, besides the arrival of the Stoneley wave, again fluid wave event E1 can be distinguished.

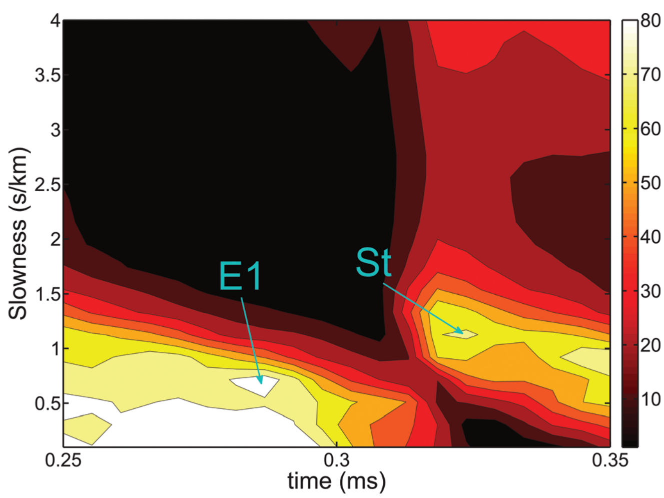

FIG. 13. Coherence plot for wave identification in the porous sample. Both Events E1 and St are clearly identified.

In Fig. 14, one pressure snapshot at 48 mm from the sample top is plotted. In the plot, the results are compared with theory using three different permeabilities: 0.5 Darcy (D), 5 D, and 50 D. It can be seen from Fig. 14 that permeability around 5 D would accurately predict the measured pressure curve. The permeability was also determined in an independent falling head laboratory experiment, from which the permeability was actually found to be 15 ± 2 D. The discrepancy between the effective permeability of 5 D and the actual permeability of 15 D can be attributed to the fact that in the theory so far only low-frequency viscous effects are incorporated, whereas also high-frequency tortuosity effects need be taken into account. Moreover, due to long residence times of the sample in the water-filled shock tube, we measured that fouling of the borehole wall decreased permeability over time. We thus argue that the permeability from the separate falling head test was probably too high.

VI. CONCLUSIONS

Tube waves are strongly affected by fractures intersecting the borehole. A theoretical description for both porous samples and fracture zones is given based on the introduction of an effective borehole fluid bulk modulus. This effective fluid bulk modulus contributes to the wave attenuation through the borehole wall impedance. This impedance can be calculated for both porous and fracture zones adjacent to the borehole, thus predicting borehole wave attenuation, transmission, and reflection over such zones. Our shock tube setup generates borehole tube waves that are used for porous and fracture zone characterization. We use a PVC sample to introduce and vary fractures in a cylindrical sample. Shock wave experiments show that attenuation in boreholes adjacent to porous zones can be predicted by theory, although the permeability fit still has a significant discrepancy. The reflection and transmission of borehole tube wave over 1 and 5 mm fractures are correctly predicted by theory, thus showing the potential of borehole wave experiments for fracture detection and characterization.

ACKNOWLEDGMENTS

H.F. would like to thank China Scholarship Council for Ph.D. fellowship support, and appreciates the technical assistance of Jan Etienne and Karel Heller. The valuable discussion with Evert Slob, Gabriel Chao, and Karel van Dalen are gratefully acknowledged.

[1]B. E. Hornby, D. L. Johnson, K. W. Winkler, and R. A. Plumb, "Fracture evaluation using reflected Stoneley-wave arrivals," Geophysics **54**(10), 1274–1288 (1989).

[2]S. Kostek, D. L. Johnson, and C. J. Randall, "The interaction of tube waves with borehole fractures, Part I: Numerical models," Geophysics **63**(3), 800–808 (1998).

[3]S. Kostek, D. L. Johnson, K. W. Winkler, and B. E. Hornby, "The interaction of tube waves with borehole fractures, Part II: Analytical models," Geophysics **63**(3), 809–815 (1998).

[4]L. Qobi, A. Kuijper, X. M. Tang, and J. Strauss, "Permeability determination from Stoneley waves in the Ara group carbonates, Oman," GeoArabia **6**, 649–666 (2001).

[5]H. Saito, K. Hayashi, and Y. Iikura, "Detection of formation boundaries and permeable fractures based on frequency-domain Stoneley wave logs," Explor. Geophys. (Sydney) **35**(1), 45–50 (2004).

[6]X. M. Tang and C. H. Cheng, "A dynamic model for fluid flow in open borehole fractures," J. Geophys. Res. **94**(B6), 7567–7576, doi:10.1029/JB094iB06p07567 (1989).

[7]G. Chao, D. M. J. Smeulders, and M. E. H. van Dongen, "Shock-induced borehole waves in porous formations: Theory and experiments," J. Acoust. Soc. Am. **116**(2), 693–702 (2004).

[8]G. Chao, D. M. J. Smeulders, and M. E. H. van Dongen, "Measurements of shock-induced guided and surface acoustic waves along boreholes in poroelastic materials," J. Appl. Phys. **99**, 094904 (2006).

[9]D. M. J. Smeulders and M. E. H. van Dongen, "Wave propagation in porous media containing a dilute gas-liquid mixture: theory and experiments," J. Fluid Mech. **343**, 351–373 (1997).

[10]R. W. J. M. Sniekers, D. M. J. Smeulders, M. E. H. van Dongen, and H. Van der Kogel, "Pressure wave propagation in a partially water-saturated porous medium," J. Appl. Phys. **66**, 4522–4524 (1989).

[11]K. W. Winkler, H.-L. Liu, and D. L. Johnson, "Permeability and borehole Stoneley waves: Comparison between experiment and theory," Geophysics **54**(1), 66–75 (1989).

[12]X. M. Tang and C. H. Cheng, "Borehole Stoneley wave propagation across permeable structures," Geophys. Prospect. **41**(2), 165–187 (1993).

[13]S. K. Chang, H. L. Liu, and D. L. Johnson, "Low-frequency tube waves in permeable rocks," Geophysics **53**(4), 519–527 (1988).

[14]D. L. Johnson, J. Koplik, and R. Dashen, "Theory of dynamic permeability and tortuosity in fluid-saturated porous media," J. Fluid Mech. **176**, 379–402 (1987).

[15]V. Korneev, "Slow waves in fractures filled with viscous fluid," Geophysics **73**, N1–N7 (2008).

[16]V. Korneev, "Low-frequency fluid waves in fractures and pipes," Geophysics **75**, N97–N107 (2010).

[17]C. V. Kimball and T. L. Marzetta, "Semblance processing of borehole acoustic array data," Geophysics **49**, 274–281 (1984).

[18]J. G. Van der Grinten, M. E. H. van Dongen, and H. van der Kogel, "Strain and pore pressure propagation in a water-saturated porous medium," J. Appl. Phys. **62**, 4682–4687 (1987).